# A Biomimetically Derived Method for Control of Span-Wise Morphing Wings

Benjamin J. Stacey* and Peter R. Thomas.†
*University of Hertfordshire, School of Physics, Engineering, and Computer Science, College Lane, Hatfield, Hertfordshire, AL10 9AB, United Kingdom*

**The development of novel morphing wings follows common milestones. This work presents the modelling and control of the recently proposed avian wing span-wise morphing concept. The concept primarily consists of three structural members heavily mimicking the skeletal structure birds employ for flight. This structure is actuated, through the range of motion achievable by avian, with the integration of pneumatic artificial muscles (PAMs). Arranged in antagonistic pairs, the PAMs actuate an effective shoulder joint between the aircraft and wing through 90°. As well as two joints along the wing through 110°, allowing a span-wise reduction of 75% the fully extended span. This adaptive structure is capable of supporting several different aerofoil geometries for application specific aircraft. Initially proposed with a biomimetic derived wing profile more traditional and predictable NACA aerofoils have been applied.**

**In this paper the avian wing span-wise morphing concept is modelled and with the application of inverse kinematics a control system is derived to allow simplified span-length positioning. Similarly, desired wing area is also presented as an input for the system. The model is based on PAM force models to individually model the pneumatic system driving each joint. The mechanical system of each joint is subsequently used to produce a direct kinematic model for wing tip position, and the inverse determined for control. The validity of both the model and system are experimentally tested on a fixed semi-span prototype rig of the morphing concept. Feedback is then introduced. Potentiometers are embedded into each joint to provide joint angle feedback. The tuning of the system is then presented for different dynamic responses.**

**Alongside this development experiments have been conducted into the kinematics avian employ in flight and the flight dynamics they enable. These results are presented and directly applied as parameters for the proposed system. Span morphing retraction and extension rates determined from in vivo flight data of avian, including the Common buzzard (Buteo buteo) and Harris Hawk (Parabuteo unicinctus), are achieved using the avian wing span-wise morphing concept and the proposed control system. These dynamics are used to infer the parameters of an aircraft with the concept wing used as control surfaces.**

## I. Introduction

The development of a control system is a vital part of a dynamic concepts development. A method for control is particularly important in the presentation of a morphing aerodynamic structure as the actuation of the system is the primary method of introducing the morph. The benefit of the morph directly relies on the accuracy and precision of the actuation. The method for achieving this control is the development of a model and applying a form of control using different methods, until desired characteristics are reached. Presented in this paper is this process in the context of a highly morphing structure a span-wise morphing concept developed to take advantage of the up to 100% morphing of avian wings. The concept utilizes highly non-linear pneumatic artificial muscles (PAMs) arranged in two dependent pairs of antagonistic muscles, allowing actuation of three revolute joints. These joints form the kinematic structure of the wing and an inverse kinematic model of this mechanical system is presented in series with and actuator model. Derived from previous works this model produces a wing tip position with 2 DOF, then related to wingspan and sweep angle. The control system is then derived using conventional methods. However, the desired dynamic system characteristics are determined through the observations of avian wings. In vivo kinematic data was captured from birds in flight using inferred motion capture tracking markers positioned on the avian body and wings. This data is then analyzed to produce

*Lecturer, School of Physics, Engineering, and Computer Science, College Lane, Hatfield, Hertfordshire, AL10 9AB, United Kingdom
†Senior Lecturer, School of Physics, Engineering, and Computer Science, College Lane, Hatfield, Hertfordshire, AL10 9AB, United Kingdom

the dynamic response of the bird wing during different types of extension. Finally in this paper, the PAM system is matched to reproduce the characteristics of the avian studied.

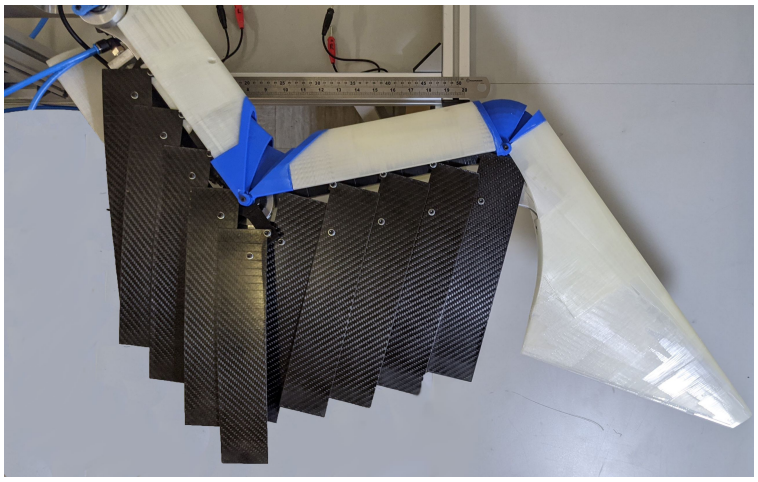

**Fig. 1 An image of the span-wise morphing concept including a concept for an articulated skin structure. Top left shows joint number one followed by the first member this continues through three of each up to the wing tip.**

Primarily, research in the field of in vivo avian has focused on aerodynamics independent of control and stability as these aerodynamic forces more directly affect efficiency. Pennycuick [1] along with others [2] have presented research into the characteristic of avian muscle to compare to the power output of birds [3]. However, similarly to aerodynamic analysis the methods avian employ for control have also been measured and modelled. Taylor et al [4], have conducted position tracking experimentation on in-flight birds using photogrammetry and inertial measurement units (IMUs). These methods both provide the angular positions, velocities, and accelerations necessary to begin to produce a model. Shepherd et al [5] used the measurements to produce rigid-body, linear state-space models using Observer/Kalman Filter identification. These models used inputs states from the tail of the avian and was limited by the values an IMU can produce; assumptions were therefore made to allow for this incomplete data, consequently the longitudinal axis was limited to 3 states. The method of measurement used for this program of work is a 'motion capture' system commonly used to capture the kinematics of animals and human. Kinematic capture allows full position tracking of points on an avian in flight, thus with correct marker placement full longitudinal and lateral modes can be assessed.

**Fig. 2 Left, female Common Buzzard Buteo buteo, approximately 1kg. Right, male Harris Hawk Parabuteo unicinctus, approximately 0.7kg. Shown are the markers; the outer wing markers are obscured and not visible in the images.**

Pneumatic artificial muscles are highly non-linear resulting in difficulties in their modeling. However, the advantage of PAMs in other aspects such as low system complexity and low weight at the point of use has driven research into effective modeling and control. The pneumatic artificial muscles referred to in this study are commonly denoted as 'Mckibben' muscles, and consist of an elastomeric bladder sheathed inside a braided fiber cylindrical sleeve affixed at both ends. The complexity in modelling PAMs both statically and dynamically derives from the interaction between

the bladder and sleeve and the internal friction produced in the braid. These stresses alongside the elasticity of the bladder are non-negligible and as such, few comparisons can be drawn between PAMs and traditional rod actuators. The conclusion of a review into methodologies of PAM modeling is that there is currently no definitive consensus on an appropriate approach to modelling of PAMs and that an ideal model may not be achievable [6]. The current state of PAM modeling therefore is one of iteration and refinement.

## II. Pneumatic Artificial Muscle System Modelling

The common elements for a dynamic system are detailed in figure 3. The sections of the system to be modeled are divided into three parts for modelling. A pneumatic system consisting of the control valve, the PAM characterization equations themselves, and the mechanical system consisting of the morphing wing structure.

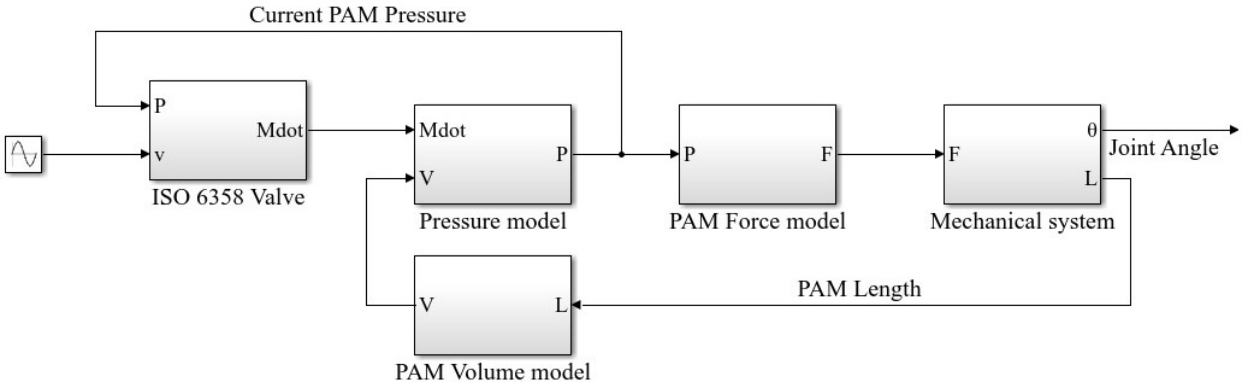


**Fig. 3 Proposed PAM model overview, outlining the sequencing of the individual component equations.**

The characterization of the pneumatics is generally based on the pressure and changing volume models of traditional ridged rod cylinders and the orifice valve models used in the representation of the control valves. The control valve selected for the morphing concept is the Festo MPYE-5-1/8-HF-010-B three state proportional control valve. Selected for several characteristics which suit the whole system. This valve also has a significant amount of literature both from the manufacture and due to other studies in the control of PAMs [7]. The nature of the spool dictating the flow results in operationally restrictive depressurization. Essentially meaning both, each of the PAMs pressurized and each PAM de-pressurized, are states that cannot be physically achieved. Others [6], have proposed implementing separate proportional valves. However, this solution is presented in applications where weight and system complexity, and by extension failure modes, are not as significant in the design as in the development of aircraft. It has been shown that the standard ISO 6358 mass flow model effectively reproduces that behavior of the Festo MPYE valve. These relate the gauge pressure of the pneumatic source and the proportionally controlled valve cross sectional area. To the mass flow rate into and exiting each muscle. Outlined in 1 where, $C$, the sonic conductance of the valve and $p_{critical}$, the critical pressure ratio are derived from or supplied by, the manufacturers literature respectively. However, to reduce computation it has been shown effective to discount the laminar case. As due to the operating conditions laminar flow is seldom present. Implemented into the system was the reduced form 2, also assuming no temperature change across the valve. In the case of the sonic conductance the reverse was employed. The method chosen for deriving sonic conductance, allowed for correlation between the spool displacement from a central position. This is preferable to other methods used for this control valve, as the displacement can be inferred from the input control voltage. This is opposed obtaining this relationship through study of the MPYE valve literature provided by the manufacture. The advantage is to reduce any error occurred from this process, however, as stated before this results in a small computational cost. The method takes the input control voltage between 0 – 10V to output a spool displacement and orifice cross sectional area. This area can be used in the modified valve model, along with spool displacement which determines the flow direction, to output the mass flow rate.

$$\dot{m} = \begin{cases} C\rho_0 \left(\frac{P_{out}-P_{in}}{1-p_{laminar}}\right)\sqrt{\frac{T_0}{T_{in}}}\left[1-\left(\frac{p_{ratio}-p_{critical}}{1-p_{critical}}\right)^2\right]^m \\ C\rho_0 P_{in}\sqrt{\frac{T_0}{T_{in}}}\left[1-\left(\frac{p_{ratio}-p_{critical}}{1-p_{critical}}\right)^2\right]^m \\ C\rho_0 P_{in}\sqrt{\frac{T_0}{T_{in}}} \end{cases} \tag{1}$$

$$\dot{m} = \begin{cases} C_1 C_d A \frac{P_{in}}{\sqrt{T}} & \frac{P_{out}}{P_{in}} \leq p_{critical}(ChockedFlow) \\ \\ C_2 C_d A \frac{P_{in}}{\sqrt{T}}\left(\frac{P_{out}}{P_{in}}\right)^{\frac{1}{k}} C & \frac{P_{out}}{P_{in}} > p_{critical}(SubsonicFlow) \end{cases} \tag{2}$$

$$With \qquad C = \sqrt{\left[1-\frac{P_{out}}{P_{in}}^{(k-1)/k}\right]}$$

$$and \qquad C_1 = \sqrt{\frac{k}{R}\left[\frac{2}{k+1}\right]^{\frac{k+1}{k-1}}} \qquad C_2 = \sqrt{\frac{2}{R}\left[\frac{k}{k-1}\right]}$$

Literary sources where similar models have been presented, often include a tubing pressure loss model. Placed directly after the valve these account for the losses in the connecting tubing between the PAMs and valve. This has not been included in this work as in the application for small unmanned aerial vehicles which may employ this morphing concept. The likely maximum length of these connections therefore is below the threshold where these losses can be considered negligible. A pressure model for a cylinder of changing volume is common in actuated system characterization due to its applicability to fix-rod cylinders. As such the equation 3 is as presented in previous works [8]. Where the terms $\alpha_{in}$, $\alpha_{out}$, and $\alpha_{vol}$, are used in place of the heat transfer coefficient k. These terms can be estimated also shown by Richer and Hurmuzlu [8], allowing the exact coefficient to be excluded.

$$\dot{P} = \frac{RT}{V}(\alpha_{in}\dot{m}_{in} - \alpha_{out}\dot{m}_{out}) - \alpha_{vol}P\frac{\dot{V}}{V} \tag{3}$$

The variable $V$ and $\dot{V}$ denoting the volume for the individual PAM are necessary for the pressure derivation. As both are highly dependent on the current length of the PAM and subsequently, its output force. The current volume is calculated from the current length, as shown in figure 3. Equation (4) shows the static volume at rest. The internal bladder thickness volume is subtracted from the total PAM volume. Using the length $L$ the cylindrical volume is produced. Total volume of the PAM is dependent on the PAM length via the kinematics of the sleeve and the individual fibers from which it is comprised. Woods [9] proposed a method for defining this relationship, which is employed in (5).

$$V_{fluid} = V_{totalvolume} - \pi[r_0^2 - (r_0 - t_{b0})^2]L_0 \tag{4}$$

$$V_{totalvolume} = \frac{B^2 - L^2}{4\pi^2 N^2} \tag{5}$$

Where, $B$, is the individual fiber length in the helical sleeve and $N$, is the number of turns that fiber makes in the length of the PAM. As the rate of change in the volume is also required (4) is differentiated with respect to time to produce (6) and simplified resulting in (7).This method is typical in PAM characteristic determination [7]. However, as previous authors have noted it assumes a cylindrical internal PAM geometry. Any observation of these artificial muscles in use makes it clear this is not the case. The crimping at each end to the sleeve, allowing attachment to connecting hardware, results in a convex rounding end.

$$\dot{V}_{fluid} = \frac{dL}{dt}\frac{d}{dL}\left[\frac{B^2L - L^3}{4\pi N^2} - \pi[r_0^2 - (r_0 - t_{b0})^2]L_0\right] \tag{6}$$

$$\dot{V}_{fluid} = \dot{L}\left[\frac{B^2 - 3L^2}{4\pi N^2}\right] \tag{7}$$

The principle method for determining the muscle forces for each PAM is a quasistatic energy balancing method proposed and significantly developed in literature. The overall force comprising of the sum of individually determined factors laid out in a PAM force equation:

$$F_{PAM} = F_G + F_C - F_B - F_S \tag{8}$$

A Gaylord force model, the most commonly employed, derived by Gaylord [10] alongside the pioneering of the muscles themselves. Developed from this initial kinematic equation Schulte [11], later Tondu and Lopez [12] and Kang et al [13], the form shown in (9). In terms of Length, $L$, PAM diameter, $D$, and sleeve braid angle, $\alpha$.

$$F_G = P\frac{D_0^2\pi}{4}\left[\frac{3\left(1-\frac{L_0-L}{L_0}^2\right)}{tan^2\alpha} - \frac{1}{sin^2\alpha}\right] \tag{9}$$

The three following force terms were largely collated in the series of work by Woods et al [7]. These proved effective in accurately simulating the internal forces and the subsequent effect on the overall contraction force of the PAM. Explained fully in other works, the bladder elasticity term $FR_B$ (10) a model of material hyperelasticity, negatively effects the output force. The included terms, $V_{bladder}$ & $V_{sleeve}$, representing the volume of the PAM bladder and sleeve respectively, were calculated using the same method as previously stated in 4.

$$\begin{aligned} F_B = V_{bladder}&\left[2C_{10}\left[\lambda_1\frac{d\lambda_1}{dL} + \lambda_2\frac{d\lambda_2}{dL} + \lambda_3\frac{d\lambda_3}{dL}\right]\right. \\ &+ 2C_{01}\left[\lambda_1(\lambda_2^2+\lambda_3^2)\frac{d\lambda_1}{dL} + \lambda_2(\lambda_1^2+\lambda_3^2)\frac{d\lambda_2}{dL}\right. \\ &\left.\left.+\lambda_3(\lambda_1^2+\lambda_2^2)\frac{d\lambda_3}{dL}\right]\right] \end{aligned}$$

$$with \tag{10}$$

$$\lambda_1 = \frac{L}{L_0}$$

$$\lambda_2 = \frac{r-\frac{t_b}{2}}{r_0-\frac{t_0}{2}}$$

$$\lambda_3 = \frac{t_b}{t-0}$$

$$F_C = -k_f(F_G + F_B - F_S)sgn(\dot{L}) \tag{11}$$

$$F_S = V_{sleeve}\frac{1}{E_s A_s^2 n^2}\frac{4\pi^2P^2B^2}{(2\pi N)^4} \tag{12}$$

Notable points include the reductive nature of all the additional terms. Including the Coulomb friction, which comprises the other force terms and a friction factor, $k_f$. Which is experimentally derived to fit and corrects for the internal material friction. This friction, mentioned previously, is a contributing factor to the complexity in modelling PAM behavior. The two PAM forces for the antagonistic system were then linked to the output angle $\theta$ through the moments about a pivot which forms the joint, then a second-order dynamic equation.

Overall the modelling of these subsystems and the Pneumatic artificial muscles themselves could be considered developed. As mentioned previously while no methodology has been definitively adopted, it is plain that a structure exists. The focus can therefore be considered to have shifted from the muscles themselves to the systems into which they are embedded. It must be noted significant progress in the form and operation of PAMs will require continued modelling development. However, for the application presented in the form of morphing structures the current orthodoxy as been proven reliable. The systems surrounding the muscles are highly adaptive allowing the range of applications. It is these applications need an approach specific to aircraft and in particular morphing aircraft.

### A. System Identification

Alongside the necessary model validation it was decided a process of frequency response would be undertaken. It was noted that the model in and of itself may not provide a reliable bases for development beyond the scope of this work. The addition therefore of a system identification methodology would support the model as development of the span-wise morphing concept developed. The production of a simplified model variant was also an aim of this process as the literature models can be computationally intensive.

#### *1. Single Frequency Response*

It was decided that a single joint dynamic control would be the most effective method for initial control. The mechanical design for the joints themselves is relatively known in literature but a few features are notable from the perspective of individual joint control. The antagonistic nature of the joint results in markedly different behaviour to the unconstrained muscles. In a context of applied an constant weight or other controlled loading situation variables such as: contraction length, internal pressure, bladder stresses, and diameter are predictably independent or dependent. Resulting in a static case. In a tension or bidirectional force connecting mechanism PAMs in a pair apply a noticeably dynamic load. This effects the performance of the muscles, reducing operating characteristics. Similarly, these must be taken into account in a control context.

The flowrate is determined by the proportional control valve as shown in the model that is then output to both PAMs. This connection, also shown in figure 4, acts as both an inlet and outlet for the PAM. The muscles themselves are affixed via threaded endcaps to a mounting plate and then to the bell crank via eye fixings, allowing for the degrees of freedom required to avoid over straining the system.

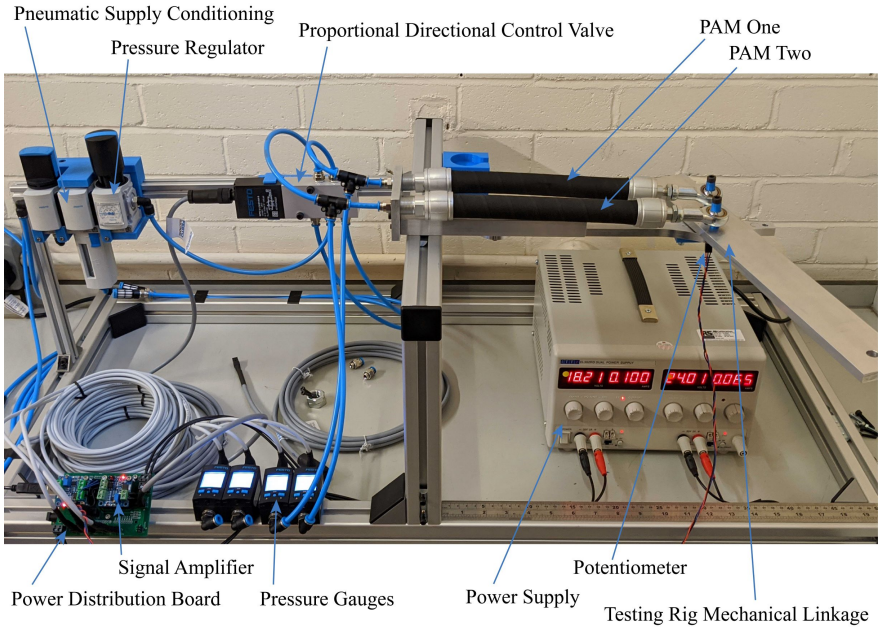


**Fig. 4 An image of the electro-pneumatic setup used for model validation and the process of frequency response system identification. Not shown is the computer providing the voltage input and recording the response. It should also be noted that this equipment rig has duplicated items for the two joint actuation of the full span-wise morphing concept.**

The underside of this joint has an embedded potentiometer providing the feedback to the micro processer. The microprocessor itself utilizes amplifying circuits to provide the control signal required by the PCV. The PAMs used in these tests were Festo DMSP. Each with a working length of 300mm and an external sleeve diameter of 20mm.

An initial set of measurements were taken with a sinusoidal voltage input of amplitude 5V about the median voltage for the control valves. Also carried out was the same test but at a range of operating pressures up to a maximum 6 Bar, defined by the maximum working pressure of each PAM. Note, the standard units for the PAMs and pneumatic equipment is bar equivalent to 100 kPa. This range of pressures and the effect on the PAM joint actuation is perhaps

best exemplified in figure 5; shown with 20mm diameter muscles. The antagonistic nature of the joint resulting in the angular defection of the joint being directly proportional to the operating pressure. Similar to linear actuation in which the contraction length is related to the contraction strain.

The implications of this in relation to the span-wise morphing concept are particularly significant. The maximum span morphing is entirely dependent on this angular defection. It is evident from these results that the defections indicated during the development were not applicable. This is due to the antagonistic PAM, the PAM that is required to extend as a result of the active muscle's' contraction, exhibiting a significantly increased resistive force than predicted. The result, a reduced actuation strain.

As the forces produced by the PAMs are related to a number of characteristics on the muscle design re-evaluation would be required for their application in situation where these characteristics, and by extension the force, are impacted due to the nature of the concept objectives. In the case of the span-wise morphing concept the primary effected characteristic is PAM volume; more significantly length. Change in length of the PAM due to the pressurisation of the bladder

It can be noted from equations 10 and 12 both sleeve volume and internal-bladder volume proportionally effect the force of the active PAM. The application of these muscles to actuate the elbow joint of the concept requires them to be embedded inside the wing box muscle volume is noticeably restricted. It is therefore clear that the critical restriction on the span-wise morphing concept is the volume of the PAMs. The implications of these result are discussed as part of the conclusion section V.

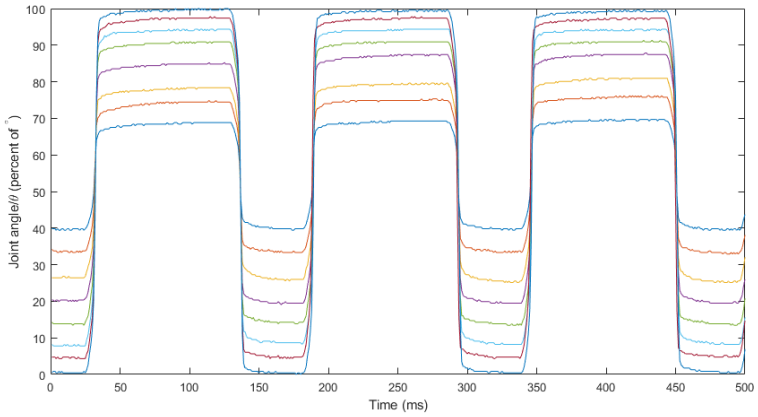


**Fig. 5 A comparison between the single pneumatic artificial muscle (PAM) joint actuated at different operating supply pressures. Shown is the measured joint angle as a percentage of the maximum angular deflection measured. This is presented as a result of a sinusoidal voltage input of 0.1 rad/s.**

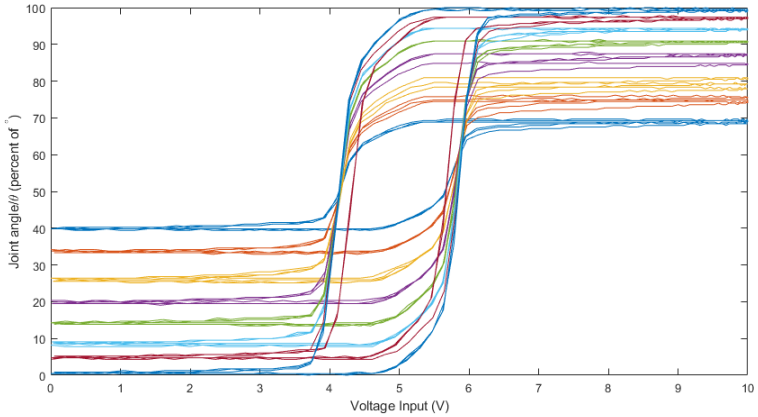


**Fig. 6 A similar comparison to figure 5. Shown against the voltage input to the proportional control valve. Of note is the significant 'dead' range away from the median voltage 5V.**

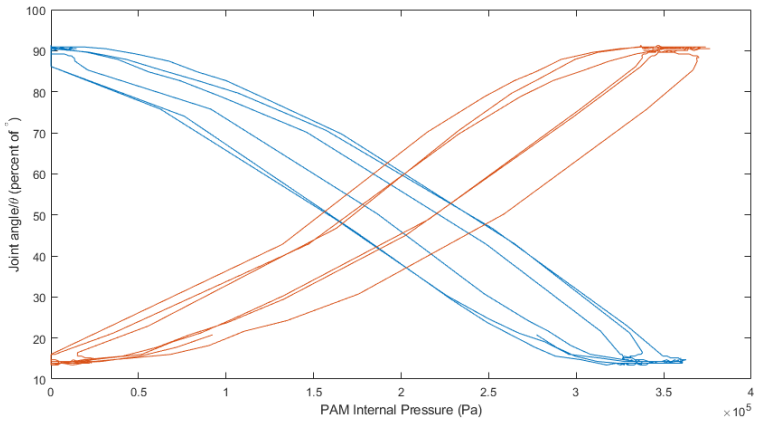


**Fig. 7 A plot showing the Internal pneumatic artificial muscle (PAM) pressure during the actuation period described in figure 5. Significant to note is the cycle formed by the pressure in the individual PAM and the inconsistent nature.**

In regards to the actuation characteristics of the single joint system a noticeable hysteresis is exhibited. Apparent in figure 6 and figure 7 it is most visible in the former. Relating the control valve input to joint angle through the range of pressures tested, it is clear the dependency of the system on its history is consistent. This consistency is seen in both the shown cycles and across the operating pressures. In comparison between the sinusoidal cycles excluding visible anomalies the joint angles are consistent to $\pm 0.5°$. The anomalies referenced are resultant from factors such as the potentiometer wire interacting with the structure of the test bench, external perturbations due to observation of the actuation, and noise that could not be filtered. The consistency in the joint angle profile as a result of the voltage input can be attributed to the manufactures tolerances for the PCV.

At a pressure of 5 bar figure 7 shows the dependency of the actuation on the interaction between the antagonistic PAMs. Over the three input cycles shown, an inconsistent behaviour can be observed. The internal pressures in each PAM can be seen to increase and decrease at a different rate over the cycles. However, as stated before it is the combined resultant force between the pair that effect the angular output. These inconsistencies therefore can be considered inconsequential. Indeed, at alternate operational pressures a greater variation in pressure can be observed. This lack of effect on the output can be observed by noting that in a cycle with a decrease pressure in PAM A, a similar decreased pressure is also observable in PAM B. The difference in the summation of the forces is therefore equal to other cycles.

As the technical documentation for the components specified there is a significant response-less region. Input voltages outside a centralised voltage range $3V < \text{Input} < 7V$ have a negligible effect on PAM actuation. While this was expected an effect on system performance was unforeseen. The microcontroller via a signal amplifier was used to drive the PCV. This controller runs an 8bit system resulting in voltage step increases to the PVC. The total number of steps is therefore limited to 255. When this was used across the full 10V range it resulted in a voltage step resolution which was detrimental to the operation of the system. This was corrected and the voltage range limited to 4V or less in subsequent system development.

*2. Frequency Response*

Frequency response testing consisted of a sinusoidal input signal amplitude 5V and amplified producing a system input voltage range from 3 – 7V. As the micro-controller produces a standard 8 bit PWM signal to the amplifiers, this voltage is stepped to 255 increments. The frequency ranges used were 0.1 rad/s to 100 rad/s. The lower bound of the frequency range was determined by the lowest angular rate measured in the avian captures. The lower limit was also chosen to represent a low manoeuvre speed. The upper limit ranging to the theoretical limit of the PAMs. This limit is determined by the mass flow rate achievable by both the flow supply and the rate achievable by the PCV PAM side orifice. It should be noted that the mechanism is not the limiting factor in actuation frequency as the amplitude of the PAM, and subsequent angle, defection decreases with frequency.

The experimental system setup for these frequency response tests, displayed in figure 4 was identical to the system used for the previous single frequency actuation. However, the attached laboratory pneumatic system was regulated down to an input pressure of 3 Bar. This pressure was selected as it produces a good compromise between the range

of motion achieved by the PAMs at a higher pressure and a manageable force output to reduce angle feedback errors caused by material deflection. This pressure as set using the same indicators then used to measure the individual PAM pressures to provide a consistent gauge pressure.

Measured at a rate of 50 Hz, were the pressure in each individual PAM and the resultant angle of joint defection. Shown in figures 8 are a range of representative cycles at each frequency. A time period of 5 seconds is shown as a common x-axis to allow frequency comparison. These results are de-trended to count for shifting of the actuation midpoint. As the amplitude of actuation decreased the pint about which the actuation centred tended towards the positive angular maximum. This actuation shift occurs immediately after power is applied. At this point, despite the PCV being in an unpowered state, the negative angled PAM is retracted resulting in the joint being initially at its limit in this direction. Despite this the actuation tend to the positive maximum. Given that the joint actuation amplitude is between 5 and 1 degrees at this frequency, the situation is likely never to be in demand. However, this shift renders the joint mechanism essentially inoperable at these frequencies.

Similarly to this tendency is an oscillation of this actuation midpoint that can be observed in figure 8g through 8k. This oscillation was not removed during the data de-trending conducted and no filtering was conducted. The amplitude of this motion can be seen to vary across the frequencies but does not exceed ±2 degrees and averages at 1 degree. This could therefore be present at lower frequencies and not observable due to the increase overall amplitude and the errors involved. However, in comparison to the overall trend this movement is negligible particularly at the low frequencies at which the joint will operate.

The same process was carried out with the positive PAM retracted in the systems initial position. The same tendency toward the positive maximum was observed leading to the concussion that the shift is due to the physical setup of the system. Due to the nature of antagonistic PAM joints the number of variables that could cause this imbalance and it would be impractical to attempt to eliminate each one. It is estimated however that the pipe losses between the PCV and PAMs has the greatest influence. Factors such as pipe length, internal cross-section and surface roughness are all factors that can be effectively managed to mitigate the issue. In the application for the span-wise morphing concept two factors negated the requirement to manage the shift in actuation midpoint. The low angle amplitudes mean that the advantages of span morphing would become negligible. While the high frequencies are rarely called for in flight as explored during the avian kinematic captures.

As a result of the two tendencies, oscillation and drift, combined with significant decrease in angular deflection. Frequencies greater than 15 rad/s were not viable for effective control. The low angles and subsequent decrease in effective wing morphing were not acceptable with the compromises of more intensive control methods including non-linear methodologies. Data sets from frequency ranges 0.1 rad/s to 10 rad/s were considered for state-space control and less intensive non-linear control. However, these were found to produce models which could not maintain accuracy across the range of frequencies. Alternatively, transfer function estimation was found to allow a greater range of operating conditions to be modelled. It was also considered that these would be less computationally intensive than state-space and more effectively altered to make viable for similar joint concepts. Transfer function estimation has significant literature covering varied applications and an instrumental-variable approach as outlined by Ozdemir et al [14]. This was used for all model estimations as part of a non-linear least squares algorithm.

In figures 9 the output of five models are shown against the input data for the model estimation. The transfer function itself is shown with each plot. These differing models are due to the estimation algorithm input data. It was determined at an initial stage that the input off all the data collected simultaneously resulted in errors. These were attributed to the non-linear nature of PAM actuation particularly in antagonistic joint configurations. Variations in frequency as low as 5 rad/s in the input data could result in model estimations exhibiting these errors. The five models represent models based on individual data sets collected at a single operational frequency. All shown are single pole transfer function models. The test stand data was collated into a bode plot in order to compare to model outputs. The result of this can be seen in figure 10. The form is a typical representation of a first order model and it was found the estimated first order models matched more consistently over higher order functions.

Figure 9a is based on the data collected at 0.1 rad/s and this original data is shown against the output of each of the other estimated models. The output of the system at these low frequencies is markedly different to those of the higher. The result is the transfer functions derived perform less accurately for the low frequency output. While the models are more consistent than at higher frequencies none replicate the higher amplitudes at are produced by the PAMs. This under-estimation is a critical failure for this method of modelling the system. The increased actuation strain of the joint and morphing concept provides control and efficiency advantages and inaccuracy in this area makes the model unsuitable at these low frequencies. An argument could be made that the low angular rates represented at this frequency would seldom be exhibited in the application of the joint in a morphing wing. This is consistent with the increased

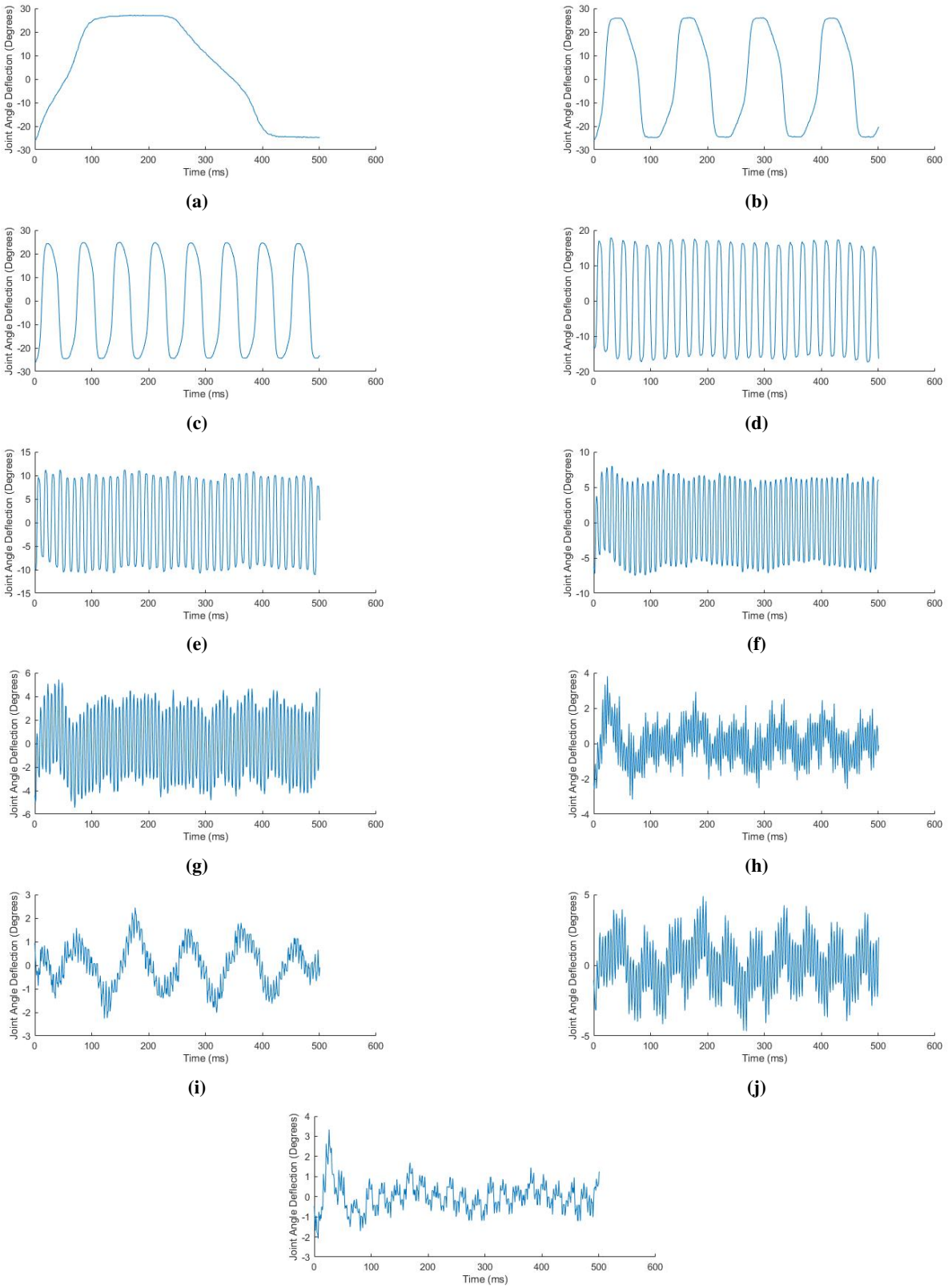


**Fig. 8 The joint angle response to a sinusoidal voltage input at the following frequencies: (a) 0.1 rad/s, (b) 0.5 rad/s, (c) 1 rad/s, (d) 3 rad/s, (e) 5 rad/s, (f) 7 rad/s, (g) 10 rad/s, (h) 15 rad/s, (i) 25 rad/s, (j) 50 rad/s, and (k) 100 rad/s. A constant amplitude was input, however, the resulting data was de-trended over the 5 seconds shown.**

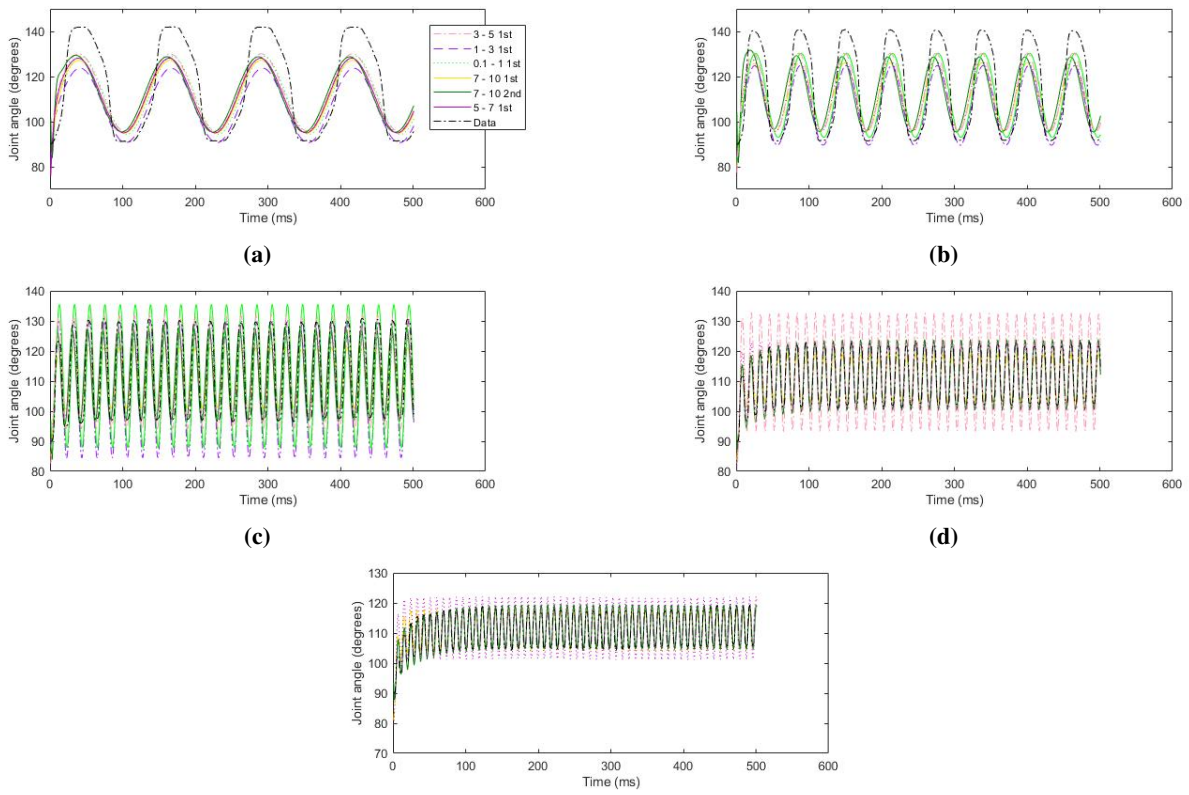


**Fig. 9 Presented are the models estimated from the PAM sinusoidal response from each of the following frequency ranges. (a) 0.1 rad/s to 1 rad/s, (b) 1 rad/s to 3 rad/s, (c) 3 rad/s to 5 rad/s, (d) 5 rad/s to 7 rad/s, and (e) 7 rad/s to 10 rad/s. Plotted at each frequency range is the output from each derived model against the following input frequency. (a) 0.5 rad/s, (b) 1 rad/s, (c) 3 rad/s, (d) 5 rad/s, and (e) 7 rad/s.**

control surface rates commonly required or MUAVs but may not be directly comparable to a full wing morphing surface. A good comparison could be made with the kinematics of the avian and the rates employed in biological flight. This is conducted in the context of the control system in section III where all the aspects of the PAM actuation is compared to in vivo captured avian kinematics.

An input at 1 rad/s to 3 rad/s produces a similar output from each model. The notable difference is a reduction in consistency between the models. Figure 9c, representing the model output at 3 rad/s, exhibits a consistent tendency that becomes apparent at increased input frequencies. Models based on low frequency data sets, in this case 0.1 – 1 rad/s, start to overshoot the experimental PAM amplitude at higher input frequencies. This is particularly evident in figure 9d where the model based on results at 1 rad/s to 3 rad/s overshoots 50% and lower models have been omitted as they could not be plotted with sufficient detail.

Models based on ranges 5 rad/s to 10 rad/s are shown to have a significantly increased accuracy and precision at their respective frequency ranges. While similarly preforming at the lower bounds examined within the scope of the joint and its applications. The overall application of these models is limited. As discussed previously the modelling of PAMs themselves is non-linear and this frequency response concurs with this characteristic. The limited range of frequencies to which each transfer function can be applied is consistent with a system with inherent non-linearity. A mechanical joint featuring PAMs in an antagonistic pair is not suited for limited control methodology. However, the accuracy of each model within its limited range has its applications in the control of the morphing concept presented. While avian vary angular rates to suit the situation, aim, and environment in the particular manoeuvres and operations, some consistent angular movement was observed. Extended through to the span-wise morphing concept this is the bases of further application into the use of these models.

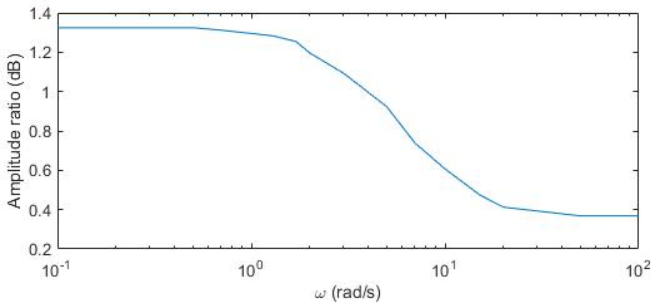


**Fig. 10 Bode plot of the frequency response system identification.**

## III. Control System

As discussed previously a three member system is used as an approximation of the avian limb. An available motion specification was three degrees of freedom to allow appropriate wing postures to be achieved. These three degrees allow the wing tip, which during derivations and calculations was referred to as the end effector, to be theoretically located at any required location. Theoretically limited by the sum of the member length, practically additionally limited by restricted angular rotation range of the joints.

The addition of the third member, for increased span over fewer members, presented an issue from a control point of view. The Kutzbach criterion defines the mobility of a system and states that the system is under constrained if the number if independent input criteria for the end effector is not equal to or greater than the degrees of freedom/mobility. The result is in order to fully define an end effector location and by extension a wing position, a third variable is required.

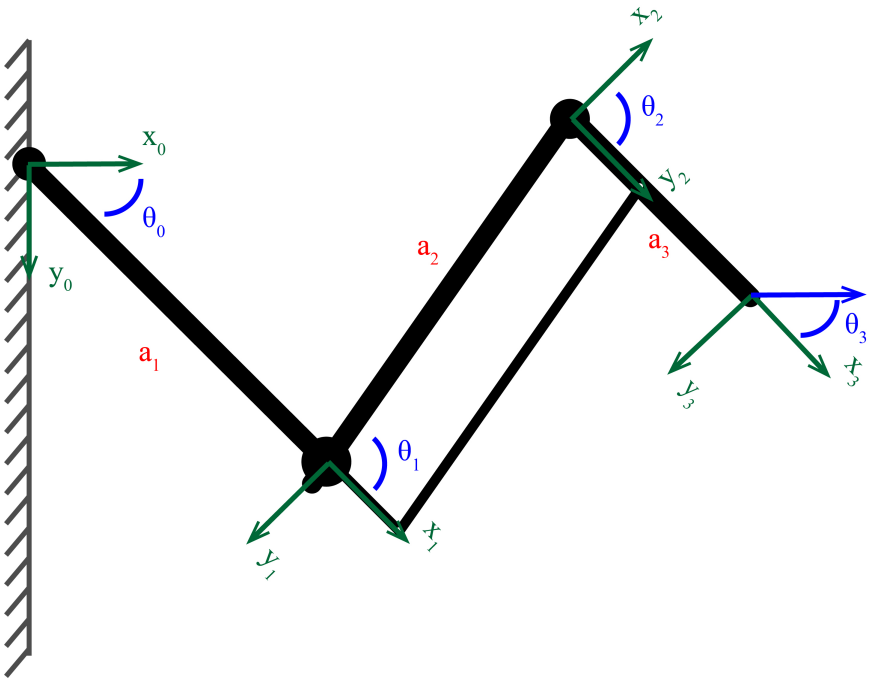


**Fig. 11 A visual representation of the notation used to define the span-wise morphing concept for application of inverse kinematics. Each linking member is denoted $a_n$ with n the end effector joint number. The coordinate systems used are also represented and similarly subscripted in relation to joint number.**

This increase in input variables introduces an advantage over alternative rotating member morphing concepts. Whilst the third variable can be of arbitrary definition in a continuation of the avian flight mechanics capture analysis, this variable represents a similar advantage avian exploit in flight. Cartesian coordinates as x and a reference value y can be taken for the longitudinal direction. The introduction of the third variable allow control over the end effector rotational

**Table 1 Values for the span-wise morphing concept proposed following the notation defined in figure 11.**

| Variable | $a_1$ | $a_2$ | $a_3$ | $\theta_0$ | $\theta_1$ | $\theta_2$ | $\theta_3$ |
|---|---|---|---|---|---|---|---|
| Value (Range) | 240mm | 270mm | 190mm | 0 - 90 | 0 - 180 | 0 - 180 | 0 - 90 |

angle about the z axis. This angle, defined as theta, can be directly related to sweep angle. In the general system case it is equal to the sweep angle of the final member but in the specific case of the span-wise morphing concept presented theta can also be used to derive the overall sweep of the wing. It should be noted that due to the parallelisms inherent in the simplification of the mechanical mechanisms used these two sweep angles are commonly equal.

Exploration of multiple version of a control system was conducted. The requirement for sweep control could be considered unnecessary in limited applications and a potential source of manual or system error. A single variable input for the system allows for a simplified control of the wing. It also allows for a more analogues application of avian flight data in the replication of flight manoeuvres. This single input was determined to be the span-length or semi-span length. A quasi-static set of kinematic equations in addition is therefore a requirement for useful application of the overall system.

Inverse kinematics for this morphing concept was completed though manual analysis of the members and joints. Several steps were taken during the mechanical development to enable a non-extensive process. This included the joint type as simple one dimensional joints and a position inline with linking members.

The coordinate systems are related to the geometry of the previous linking member from the ridged joint. Detailed in figure 11 is the related notation. The inverse kinematic equations follow this in order of computation effectively from the end effector to the ridged body. Input; $x_3$, $y_3$ and, $\theta_3$, the position of the wrist joint is established in (13).

$$\begin{aligned} x_2 &= x_3 - a_3 c(\theta_3) \\ y_2 &= y_3 - a_3 s(\theta_3) \end{aligned} \tag{13}$$

In relation to the position of the wrist joint and its coordinate system, the derivation of $\theta_2$ the secondary actuated joint can be completed. Via the assumption of the member geometry a value, $Z_1$ , for the $a_1$ and $a_2$ member angle can be ascertained. Equations, (14) and (15). An assumption was made regarding the members relationship in order to reduce the variables. This process assumes the members $a_1$ and $a_2$ are constrained at an angle less than parallel. This is the case for the span-wise concept as presented but it should be noted as a possible cause for error in any future development.

$$r_{12} = \sqrt{x_2^2 + y_2^2} \tag{14}$$

$$Z_1 = c^{-1}\left(\frac{r_{12}^2 - a_1^2 - a_2^2}{-2a_1 a_2}\right) \tag{15}$$

$$\theta_0 = \theta_3 \tag{16}$$

$$\theta_1 = 180 - Z_1 \tag{17}$$

These simplified equations allow a computationally light response to manual input. However, and perhaps more significantly, this system allows for a more concise control approach. System specific values for joint angles and their subsequent motion and aerodynamic and stability impact, are not required. The total area within which the end effector can be located is highly dependent on the rotational range of the individual joints. The most impactful on the x span position is the shoulder. In an ideal mechanical situation theta the shoulder angle would range from +45 to -45 corresponding to perpendicular with the body of the aircraft to parallel. In the context of high manoeuvrability, high velocity aircraft forward swept wings, in this case greater than +45 could also be considered. Dictated in the inverse kinematics, it can be seen that the elbow joint thi has a less significant impact on the range of motion of the end effector. This can justify the any mechanical shortcomings in the physical design due to the additional constraints of parallel system integration.

## IV. Biomimetic application

Presented in this paper thus far is what could be considered a generic mechanism for control of the morphing wing. Used is combination of both the dynamic PAM joint control and the inverse kinematics for wing tip positioning and an accompanying direct kinematic model for manoeuvre simulation. These allow common inputs, wing tip position and angle of attack, to be used for system level control. However, there is a requirement for a higher level of control which removes the requirement for system level interaction. The proposed additional set of equations allowing this is based upon the joint relationships measured during the avian kinematic capture. Replication of these relationships allows the concept to utilise the unique motion characteristics of the avian and allow adaptation based on manoeuvre and behaviour analysis collected from motion capture. The primary motion of the concept is the extension in the span-wise direction. This was taken forward and the each of the other input variables defined in relation to the span.

A number of avian flight modes were explored and as the full extension and retraction of the wing occurs as part of each flight, it would be impractical to incorporate each one. These full extensions are most common in the take-off of the bird from a perch, as a method of stability on an unstable perch, and during ground locomotion. It was observed that in each of these instances a three-dimensional motion was exhibited. In application to the span-wise morphing concept the two-dimensional reduction of the movement was considered. This reduction simply omitted the z-axis and calculated joint angles based on the span and chord motion.

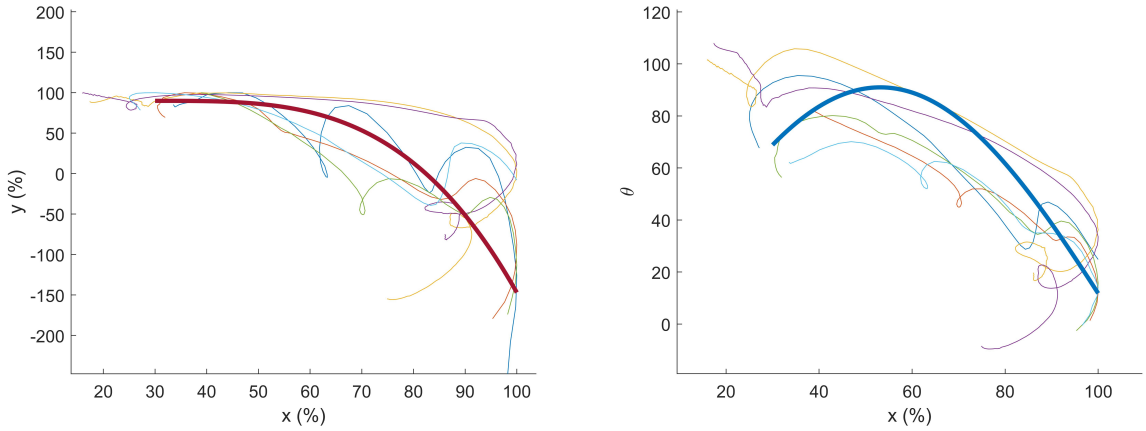


**Fig. 12 (a) Avian motion capture data showing the chord-wise $y$ positions of the wing tip as a percentage of the maximum $y$ position. Against the $x$ position of the wingtip similarly as a percentage of the maximum value for span position. Also shown is the derived curve used to approximate the relationship between the two variables. (b) Presented as the angle of attack against the span-wise position $x$. Similarly shown is the curve used to define the angle of attack $\theta$ as a function of span.**

Complicating matters further there is an argument to similarly including partial extensions and retraction when considering the motion, as opposed to the full. Any control system based on the avian kinematics measured will be required to operate full wing actuation. However, it is reasonable that the partial actuation shown in flight could be extrapolated for the control though the entire range of motion. It was considered that the kinematics captured mid-flight, as opposed to a full extension from rest at take-off or similar, may benefit the control of the span-wise morphing concept to a greater extent. Several reasons for this are evident. While mid-flight the aerodynamic consequences of perturbations are increased due to the high airspeed. This could result in the more aggressive actuation used at low or no airspeed causing instability in the flight of the span-wise morphing concept. During flight the motion of the wings have a significantly different effect on the centre of gravity as compared to perch or ground based motion.

A compromise was made between the two kinematic data types. The full retraction kinematics explored are more numerous. This is due to the proportion of its usage during flight and the relative ease to capture extensions on take-off. A great certainty as to the reliability of the measurements can be taken for the average of all the full extension kinematic data collected. While the motion employed immediately during take off can be considered in flight with all the implications suggested previously. This is despite the bird still being in contact with the perch for a portion of the capture. Therefore, the averaging of the full extension and retraction kinematics were the bases for this proposed control

system. This compromise in motion capture selection is a clear area for further development. The development of flight mode specific control is of particular interest in further research.

The proposed input to the system is the spanwise position $x_3$ in relation to the $x_0$ coordinate system. The two variables which are to be made dependent are $y_3$ and $\theta_3$. A summary of the take-off avian data is shown in figure 12a. The plot details the $y$ position of the wingtip end-effector against the span-wise position $x$. These individual motion paths are constant despite the difference in flight conditions. The initial position of the wing tip is, as expected, the most repeated portion of the motion. While the wing is tucked into the body the wing tip is restrained in its movement. Two paths start at a greater span. This is due to poor motion capture data at the start of the wing extension as opposed to any change in the manoeuvre itself. The gradient of the initial movement starts low before increasing in general exponentially. The varied nature of the latter stages of the extension would require an increased number of captures to make any general conclusions. However, with the relatively minor impact on overall performance and the nature of bio-inspired design not being a direct copy of nature, a limited set was decided to be sufficient for the control system. Plotted in figure 12 is the curve derived from the available data. The curve is characterised through the exponential equation 18. This curve proved to provide the best approximation between the low gradient and high gradient sections of the extension. Where polynomial and similar curves less adequately represented both characteristics.

$$y = -4 \times 10^{-5} x^{3.386} + 106.5 \tag{18}$$

The angle $\theta_3$ the angle between the $x_0$ and $x_3$ axis' is the second inverse kinematic input proposed to be controlled via avian behaviour. This angle can be effectively taken to represent the angle of attack for the semi-span of the wing. Due to the linked elbow and wrist joint the angles $\theta_0$ and $\theta_3$ are equal. The selection of this as an dependent variable allows further simplification of the system through the omission of any further equations linking the variables. In a similar process to the y variable, figure 12b exemplifies the relationship between the x span position and theta. These were again taken for the previously mentioned bird flights. These plots show a more defined profile for the motion. Each flight consistently used a curved profile at the start and end of each movement. While the central portion of the motion can be considered more or less linear. The motion capture does show a repeated pattern however, there are several notable exceptions. The beginning and end of each motion is not consistent, while the curve is similarly undefined in terms of x value position. In a similar fashion to the y position plots the theta angle does exhibit a highly repeatable gradient against the span position. This can therefore be the feature from which the dependency can be derived.

It was decided no to relate the two variables linearly. A linear relationship would compromise the accuracy at the maximum and minimum retraction positions where the curved profile is most pronounced. A polynomial based equation was considered and it was found at 3rd order or greater a reasonable curve was produced. However, these tended to produce low theta angles at lower $x$ position values. This was deemed too significant a deviation to be considered. The equation 19 was produced from a sine based curve fit. This provided the most reliable fit over the full range of span values. However, in plot 12b it can clearly be seen this is a compromise over the range too.

$$\theta = 91 \sin(0.02175x + 0.8365) \tag{19}$$

The method by which both of these dependencies were derived is fundamentally variable. The curves presented as a solution in this case are suited for this type of structure actuation. However, it is clear that the method is easily applied to differing situations. A similar process could be undertaken, using the same methodology, for wing twist, camber, and chord length. On the span-wise morphing concept this technique could be utilised for the effective control of wing sweep through the analysis of avian such as the Swift that use sweep angle extensively in flight.

### A. Control validation

In a similar method to the single joint experimentation explored in section II.A, a rig was constructed to validate the controlled system. Two actively controlled joint and a single passive joint was constructed from aluminium plate with initial weight reduction included for validation purposes. In previous loadings with each muscle at 6 bar elastic deformation of the members was observed. It was predicted that deformation within the material strength would affect the angle feedback causing instability. This was mitigated with the application of a high-grade 7071 alloy. The pneumatic artificial muscles themselves were mounted in orientation to their respective joint though embedded threaded fittings.

The inboard PAM set, shown in figure 13, are intended to housed within a fuselage to mitigate aerodynamically adverse structural elements required for their containment. It should be noted that the angle about the z axis the PAMs form with the neutral position of the actuated member is critical mechanically. However, this can be obviated through

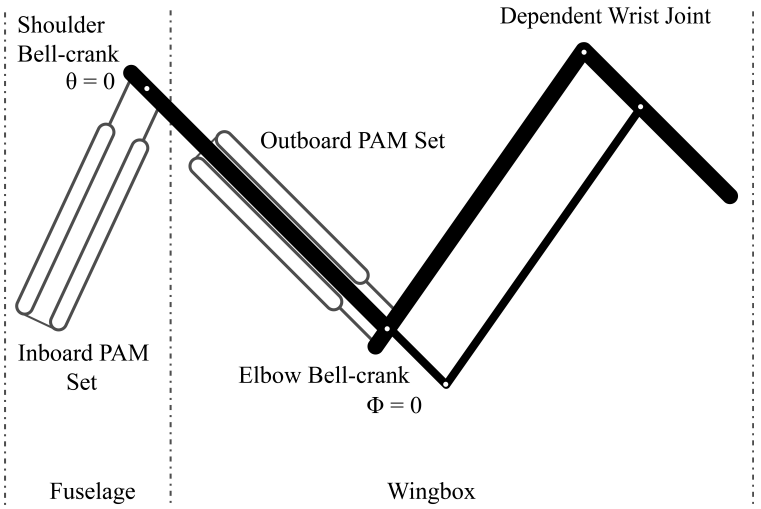


**Fig. 13 A diagram detailing the mechanical layout for the control system testing. Shown are both pairs of pneumatic artificial muscles (PAMs). Each actively actuating their respective joints with the outboard pair passively actuating the final wrist joint. Note this diagram does not represent scale.**

the mechanical linkage connecting the PAMs to the joint. As such the position of the inboard pair in figure 13 shows a possible configuration. Where as, the setup detailed in figure 14 is rotated toward the fore as this equipment was also intended for wind tunnel use and space limitations caused interference with the wing body.

In the setup image the structural fuselage analogue is visible supporting the structural members and housing the inboard PAMs. This serves only as a stand-in for an airframe mounting. The overall setup is similar to that of the single joint experimental rig shown previously. Accommodations were made for the second joint via the inclusion of a replicated set of support equipment. Pneumatically, both muscle pairs are connected to a proportional control valve MPYE-5-1/8-HF-010-B and individually pressure transducers SPAU. Electrically, both muscle sets were connected to a common power sources and for data singles a common microcontroller. The control loop described in the previous section was ran separately on a computer to allow data collection, monitoring, and adjustability. An overview of the physical system as proposed for the test and application in the span-wise morphing concept is shown in figure 14. The significant differences from the single joint testing is the duplication of the PAM support components: the PCV, Pressure sensors, and control signal amplifier.

A sinusoidal input was used to validate the control methodology chosen and the control system developed. The control system can only be considered quasi-static due to the initial basic implementation of the inverse kinematics. As a result the input value was of desired span length with the out two joint angles. While the inverse kinematics used three inputs based on the span length; as detailed in section IV. In order to explore the versatility of the mechanism tests with different muscle parameters were tested. The system was run at 8 bar with two pairs of 10mm diameter bladder PAMs. While a second configuration with the outboard joint using the same 10mm pair while the inboard joint used the 20mm valiant; this was conducted at 6 bar. This 6 bar was used due to the upper pressure limit of the 20mm PAMs. A configuration with a 20mm pair at the outboard position could not be achieved as the length of the larger pair could not be accommodated in the structure design. This has been identified as an avenue for further research.

The full set of results for this 6 bar test is shown in figure 15, over a range of three representative cycles. The first point of note is the reduced input amplitude. It was noted after analysis of the avian motion capture that solely in the extension manoeuvre the wing does not reach full retraction. This is due to taking the reference point at the centre of the body which obviously does not retract in the same manner. Similarly, it is only in further actions, such as a flapping stroke, that the avian extends past approximately 75% span. These were therefore restricted for this test of the extension exclusively.

The following control stage incudes the calculating the dependent variables according to the biomimetically derived curves. As discussed in a previous section the curves that define the relationship between the variables are so called 'best fit' for the data collected. This can therefore be considered the more adaptable section of the control system. Far from presenting a negative to the control of the span-wise morphing concept, this allows greater flexibility in the

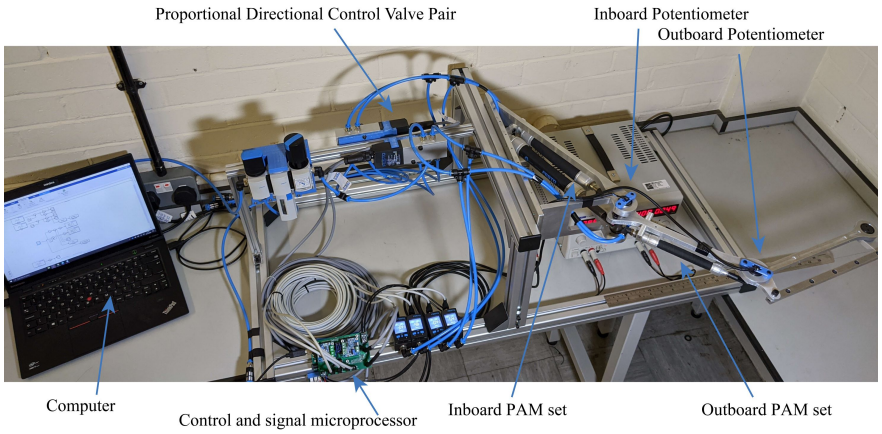


**Fig. 14 An image of the complete setup used to validate the control system in a passive environment. Labelled are the additional components which make up the three jointed system as opposed to the single joint pneumatic artificial muscle control setup. Note none of the aerodynamic surfaces of the span-wise morphing concept are present during these tests.**

application of this methodology. The figure 15b presents the output of the particular variables defined for this concept. The variable $y_3$ is characterised by a broad peak and narrow trough. This can be found typical due to the exponential relationship to the input variable. However, given the nature of the avian motion capture it is perhaps an understated response as the data showed a significant exponential y position change during retraction. It can be considered, given the nature of novel concepts, an understated response may be preferable at this stage. The flexibility in the equations allows for further development if necessary.

The variable $\theta_3$ is also shown in figure 15b. Based on a sinusoidal curve out phase with the input a more standard output is presented in comparison to the $y_3$ value. Another phase shift can be observed in the subsequent stage of the control system; shown in figure 15c. This figure shows a plot of the 'shoulder' angle and 'elbow' angle, $\theta_0$ and $\theta_1$ respectively. The phase change in $\theta_0$ is due to the axis change required for the kinematics as the reference datum changes for application to the muscles. This effectively sets the two joints out of phase. The opposing arrangement of the artificial muscles in each joint explains this system output.

The feedback angle shown in the final plot in figure 15 makes clear a limitation in the system made clear by early joint angle validation testing. The primary limit on the muscles is force and when arranged antagonistically the opposing force reduces the operation angle range. A comparison between the desired angle from the avian results/ kinematics and the measured output angle shows a noticeable difference in amplitude. An approximate average of 55% reduction in actuation strain can be observed when driven to the same joint deviations as measured from the avian used for the system.

However, mimicking avian manoeuvre behaviour precisely is only of benefit if the result is improved flight performance over current morphing UAV and MUAV concepts. The control system in comparison with existing concepts gives a similar indication of performance. It is clear from the validation testing while the amplitude is not achieved the output is defined. Each of the joint angles matches closely in phase with the input demanded of the kinematics. The output span is therefore matched through the use of a biomimetically derived quasi-static control system.

## V. Conclusion

In this paper the avian wing span-wise morphing concept was modelled and with the application of inverse kinematics a control system is derived to allow simplified span-length positioning. The model is based on PAM force models to individually model the pneumatic system driving each joint. The mechanical system of each joint is subsequently used to produce a direct kinematic model for wing tip position, and the inverse determined for control. The validity of both the model and system were experimentally tested on a fixed semi-span prototype rig of the morphing concept. Feedback is then introduced. Potentiometers are embedded into each joint to provide joint angle feedback. A method for frequency response system identification was presented for applications in deriving a experimentally derived model. This method showed limited success in the application on pneumatic artificial muscles due to their highly non-linear

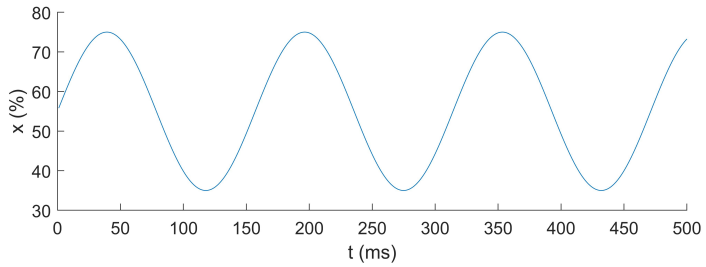


**(a) System input, span length as a percentage of maximum span length.**

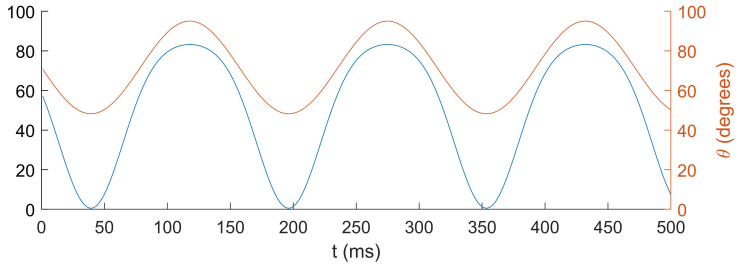


**(b) Dependent variables, $y_3$ blue, $\theta_3$ orange.**

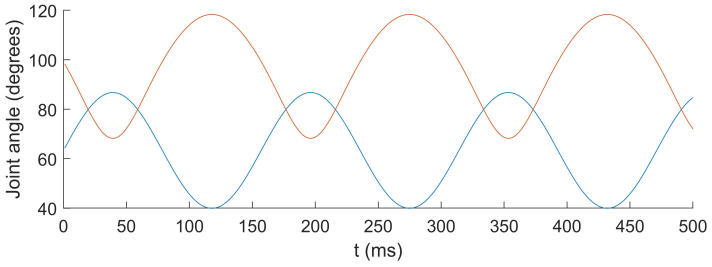


**(c) Inverse kinematic output, $\theta_0$ blue, and $\theta_1$ orange.**

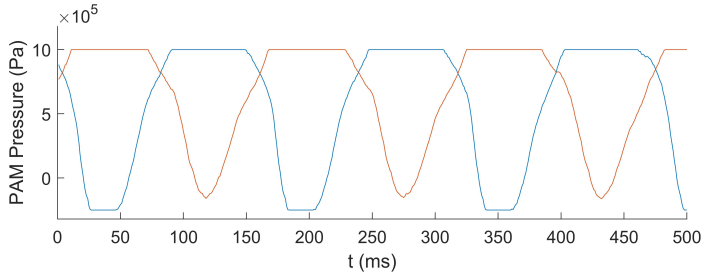


**(d) Measured Pneumatic artificial muscle (PAM) pressure, leading PAM in orange, trailing PAM in blue.**

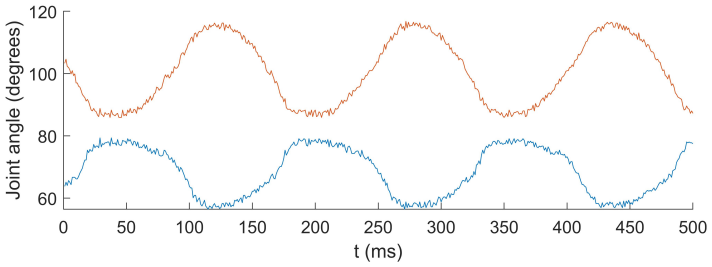


**(e) Measured Joint angles, $\theta_0$ blue, and $\theta_1$ orange.**

**Fig. 15 Presented are the outputs at each stage of the control system these form the input to the subsequent stage. (a) the system input; span position as a percent of maximum span, (b) the output of the dependent variables based on avian derived relationships, (c) inverse kinematic output joint angles, (d) resultant measured PAM pressures, (e) measured joint angles produced by the concept.**

characteristics. It was shown however, that over a narrow range of applied frequencies a relatively simple first order transfer function could provide an adequate estimation of the system response. The control system based on joint angle was deemed to be too low level for meaningful control. A method for defining dependent input variables to a single span length variable was presented. These dependent inputs would be defined through the relationships observed in similar avian flight manoeuvres. The kinematics used in the wing joints of avian were presented as measured using motion capture and the dependent variables defined. While the span-wise morphing concept cannot match the full physical range of motion exhibited by the avian studied, the control of the wing was successful. A system was presented with a single span-wise input that would reliably and accurately control the span-wise morphing concept.

## Acknowledgments

The authors would like to acknowledge the contributions to this research from the Sir Geoffrey De Havilland Fund.

## References

[1] Pennycuick, C. J., "Power requirements for horizontal flight in the pigeon Columba Livia," Vol. 49, 1968, pp. 527–555.

[2] Tobalske, B. W., "Biomechanics of bird flight," *Journal of Experimental Biology*, Vol. 210, No. 18, 2007, pp. 3135–3146. https://doi.org/10.1242/jeb.000273.

[3] Biewener, A. A., "Muscle function in avian flight: achieving power and control," *Philosophical Transactions of the Royal Society of London B: Biological Sciences*, Vol. 366, No. 1570, 2011, pp. 1496–1506. https://doi.org/10.1098/rstb.2010.0353.

[4] Taylor, G., Bacic, M., Bomphrey, R., Carruthers, A., Gillies, J., Walker, S., and Thomas, A., "New experimental approaches to the biology of flight control systems," *The Journal of Experimental Biology*, Vol. 211, 2008, pp. 258–266. https://doi.org/10.1242/jeb.012625.

[5] Shepherd, S., and Valasek, J., "Modeling and Analysis of Eagle Flight Mechanics from Experimental Flight Data," 2012. https://doi.org/10.2514/6.2012-27.

[6] Tondu, B., "Modelling of the McKibben artificial muscle: A review," *Journal of Intelligent Material Systems and Structures*, Vol. 23, No. 3, 2012, pp. 225–253. https://doi.org/10.1177/1045389X11435435.

[7] Woods, B. K., Kothera, C. S., Wang, G., and Wereley, N. M., "Dynamics of a pneumatic artificial muscle actuation system driving a trailing edge flap," *Smart Materials and Structures*, Vol. 23, No. 9, 2014. https://doi.org/10.1088/0964-1726/23/9/095014.

[8] Richer, E., and Hurmuzlu, Y., "A high performance pneumatic force actuator system: Part I—nonlinear mathematical model," *Journal of Dynamic Systems, Measurement and Control, Transactions of the ASME*, Vol. 122, No. 3, 2000, pp. 416–425. https://doi.org/10.1115/1.1286336.

[9] Woods, B., Bilgen, O., and Friswell, M., "Wind Tunnel Testing of the Fishbone Active Camber Morphing Concept," 2012.

[10] Gaylord, R. H., and Gaylord, R. H., "Fluid Actuated motor system and stroking device," , jan 1958.

[11] Schulte, H. F. J., "The Characteristics of the McKibben artificial muscle." *The Application of external power in prosthetics and orthotics.*, National Academy of Sciences-National Research Council, Washington D. C., 1961.

[12] Tondu, B., and Lopez, P., "Modeling and Control of McKibben Artificial Muscle Robot Actuators," *IEEE Control Systems*, Vol. 20, No. 2, 2000, pp. 15–38. https://doi.org/10.1109/37.833638.

[13] Kang, B. S., Kothera, C. S., Woods, B. K., and Wereley, N. M., "Dynamic modeling of mckibben pneumatic artificial muscles for antagonistic actuation," *Proceedings - IEEE International Conference on Robotics and Automation*, 2009, pp. 182–187. https://doi.org/10.1109/ROBOT.2009.5152280.

[14] Arda Ozdemir, A., and Gumussoy, S., "Transfer Function Estimation in System Identification Toolbox via Vector Fitting," *IFAC-PapersOnLine*, Vol. 50, No. 1, 2017, pp. 6232–6237. https://doi.org/10.1016/j.ifacol.2017.08.1026.